Mechanics Research Communications 69 (2015) 34–39

Contents lists available at ScienceDirect

Mechanics Research Communications

journal homepage: www.elsevier.com/locate/mechrescom

Improved shielding structure with double honeycomb cores for hyper-velocity impact☆

Ping Liu, Yan Liu*, Xiong Zhang

School of Aerospace Engineering, Tsinghua University, Beijing 100084, China

ARTICLE INFO

Article history:
Received 30 January 2015
Received in revised form 16 May 2015
Accepted 7 June 2015
Available online 16 June 2015

Keywords:
Double honeycomb cores
Internal-structure model
Hyper-velocity impact
Material point method

ABSTRACT

Aluminum sandwich panel made from double honeycomb cores can serve as a cost-effective shielding structure against hyper-velocity impact of space debris. The double honeycomb sandwich panel is improved and investigated in detail in this paper. Different from the original structure, the transverse position of the intermediate facesheet is varied instead of at the right middle of the panel. The influence of the transverse position is investigated numerically with point-based internal-structure model and material point method. Much better shielding performance can be obtained when the distance between the intermediate facesheet and the front facesheet is around the equivalent shielding distance. The equivalent shielding distance is defined as the maximum distance the debris fragments can travel in transverse direction before they interact with honeycomb cell walls. The morphologies of the facesheets and the residual energy are also discussed. A new shielding structure with multiple intermediate facesheets is suggested based on simulation results, and substantially improved shielding capability is achieved.

1. Introduction

Honeycomb sandwich panels are widely used in many engineering disciplines [1–4]. Though different forms of sandwich cores, such as aluminum foam [5,6] and Nomex honeycomb [7], have shown more attractive properties, common aluminum honeycomb sandwich panels still play an important role in engineering applications especially on unmanned spacecraft as major load-bearing components [8]. Shielding structures can also be built based on honeycomb panel to protect inside functional elements from hyper-velocity impact of orbital debris [9]. One drawback of honeycomb sandwich shielding structures is that the debris fragments are confined in a small region due to the existence of honeycomb cell walls, which is named channeling effect. Channeling effect implies concentrated impact energy flux and sequentially decreased shielding performance.

Turner et al. [9] proposed a cost-effective shielding structure, called double honeycomb panel, by simply inserting one intermediate facesheet between the front and the rear facesheets. A significant performance increase can be observed for the new shielding structure. It was reported that the ballistic limit, defined as the projectile diameter when the hole diameter of the rear facesheet equals 1 mm, increased from 0.58 mm to 0.91 mm at the cost of mass increase 1.2 kg/m^2 [9].

The shielding capability of honeycomb sandwich panel has been investigated experimentally [9] and numerically [10,11]. The ballistic limit equations were obtained based on a series of experimental results [8,12]. Different simulation techniques, such as SPH method [10] and material point method (MPM) [11], were used to investigate behaviors of honeycomb sandwich panel under hyper-velocity impact, especially for the velocity range the experiments cannot cover. Channeling effect was clearly observed from numerical results.

As a meshfree particle method, MPM is very competitive for problems of large deformation and fragmentation. No mesh distortion exists in MPM. Numerous contacts and self-contacts can be dealt with easily in MPM. Another important advantage is the high efficiency in large deformation phase, which is attributed to no decrease in critical time step size and no neighbor particle search. Ma et al. [13] compared MPM with widely-used meshfree SPH method, and they found that the computational cost of MPM can be several times lower than that of SPH. MPM has been successfully applied for high- and hyper-velocity impact problems [6,11,14–16]. One important advantage for high- and hyper-velocity impact simulation is that MPM can describe fragmentation and debris cloud

☆ Supported by National Natural Science Foundation of China (Grant Nos. 11472153 and 11102097) and Beijing Higher Education Young Elite Teacher Project (No. YETP0111).

* Corresponding author. Tel.: +86 10 62789122.
E-mail address: yan-liu@tsinghua.edu.cn (Y. Liu).

http://dx.doi.org/10.1016/j.mechrescom.2015.06.003
0093-6413/

without erosion schemes, which is quite different from traditional finite element method. Such an advantage ensures mass conservation throughout the impact process. The performance of shielding structures with aluminum foam was investigated with MPM model reconstructed from CT-scanned images [6]. MPM internal-structure model was built and used for direct simulation of high-velocity impact on single honeycomb panel [11]. Particle feature made model construction simple and straightforward. The influences of internal-structure form and parameters can be studied directly with point-based internal-structure model.

The shielding capability of improved double honeycomb structure is investigated in this paper based on MPM and internal-structure model. Material point method, material models and the double honeycomb structure are introduced briefly in Section 2. An improvement technique of moving intermediate facesheet is also proposed. Then the simulation results are given and discussed in Section 3. A much improved multilayer honeycomb structure is proposed based on simulation results. The paper is concluded in Section 4.

2. Simulation method and models

A set of Lagrangian points and an Eulerian background mesh are used in MPM. Lagrangian points trace history variables such as stress and plastic strain. The background mesh is used to solve momentum equations and to calculate spatial derivatives. MPM usually utilizes explicit time stepping scheme. At the beginning of each MPM step, a regular background mesh is established, and history variables are mapped to background mesh nodes. The momentum equations are solved on background mesh nodes. Then the variables on Lagrangian points are updated based on the increments on background mesh nodes. The above process means that Lagrangian points are bound to and deform with background mesh inside each step. At the end of the step, the deformed background mesh is abandoned. Regular background mesh is reused for the next step. Lagrangian points can overcome the challenge of interface tracking problems and convection term in pure Eulerian method. While Eulerian mesh can guarantee valid element deformation and feasible time step size which may have difficulties when large deformation is encountered in traditional Lagrangian mesh-based method. For a more detailed introduction to MPM, see e.g. Ref. [13,17].

The inherent contact algorithm in standard MPM is a non-slip contact constraint as single-valued velocity field is ensured automatically [18]. The same hyper-velocity impact example was computed by standard MPM and MPM with contact algorithms and different friction coefficients [16], and the friction coefficient was found to play a negligible role in the final morphology in hyper-velocity impact range and all the results were very close.

Detailed establishing process of internal-structure model of honeycomb core is given in Ref. [11]. The transition between facesheets and honeycomb core is straightforward and no special discretization treatment is needed. It is also convenient for MPM to refine the model to improve the accuracy and to show the details of the impact process. MPM internal-structure model for single honeycomb panel was validated in [11]. Comparisons of hole diameters and hole shapes between numerical results and experimental results or empirical formulas showed good agreements.

Double honeycomb sandwich panel is made of three facesheets and two honeycomb cores. They are the front facesheet, the intermediate facesheet, the rear facesheet, the front honeycomb core and the rear honeycomb core, as shown in Fig. 1. t_f, t_i and t_r are the thicknesses of the front facesheet, the intermediate facesheet and the rear facesheet, respectively. D_{hc} is the incircle diameter of the honeycomb cell. t_{hc} is the thickness of cell wall. S_f and S_r are distances between facesheets. d_p is the projectile diameter. Parameter values are listed in Table 1.

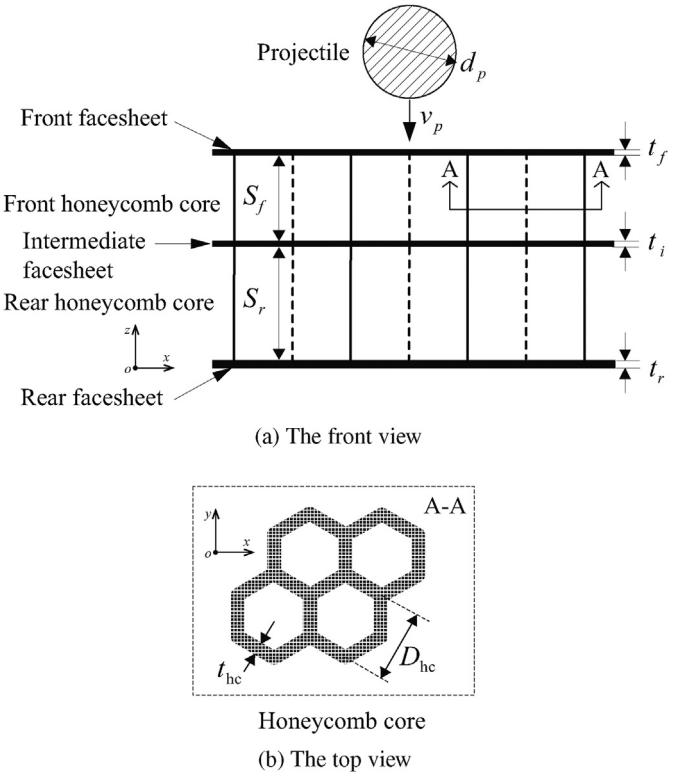

Fig. 1. Schematic diagram of double honeycomb panel.

Both the sandwich plate and the projectile are made of aluminum alloy. The facesheets are made of Al2024-T81, the honeycomb cores are made of Al5052, and the projectile is made of Al2017. All of these materials are the same as used in the experiments of Ref. [9]. Johnson-Cook strength model and Mie–Grüneisen equation of state (EOS) are adopted to simulate the metal behavior under high pressure and high temperature. The material models used in this paper are identical to those adopted in Ref. [11], where material parameter values were listed in detail. The validity of using Johnson-Cook model and Mie–Grüneisen EOS was also discussed [11].

The intermediate facesheet is moved in the transverse direction (out-of-plane direction) with an interval of 2.125 mm to investigate influences of S_f and S_r on shielding performance. The summation of S_f and S_r, that is the total height of honeycomb core, is kept at 34 mm. Hyper-velocity impacts on seventeen configurations of double honeycomb structures, including the two extreme cases where the intermediate facesheet merges with the front facesheet (S_r = 34 mm) or the rear facesheet (S_r = 0), are simulated. S_r = 17 mm corresponds to the original double honeycomb panel. As shown in Ref. [9], there is a critical impact velocity at about 6–7 km/s where the shielding performance of double honeycomb

Table 1
Geometric parameters.

D_{hc} (mm)	t_{hc} (mm)	t_r (mm)	t_i (mm)	t_f (mm)	S_f+S_r (mm)	d_p (mm)
4.76	0.178	0.4	0.4	0.4	34.0	2.0

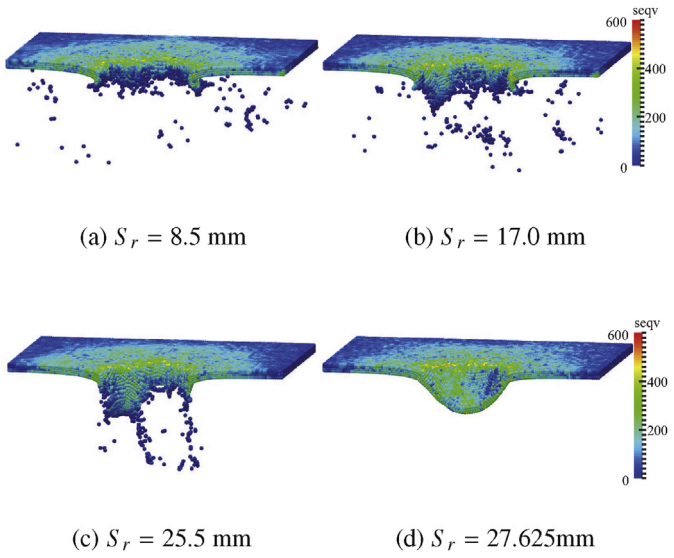

Fig. 2. Morphologies of the rear facesheets at $t = 50$ μs. $v_p = 4$ km/s.

panel changes. When the velocity is below the critical velocity, the ballistic limit increases as the velocity increases; otherwise the ballistic limit decreases as the velocity increases. In order to eliminate the influence of the critical velocity and fit for hyper-velocity impact condition, the impact velocities $v_p = 4$ km/s and $v_p = 5$ km/s are focused on.

3. Results and discussion

3.1. Final morphologies

Final morphologies of the rear facesheets are firstly studied. Morphologies of four configurations for $v_p = 4$ km/s are shown in Fig. 2. Results for $v_p = 5$ km/s are shown in Fig. 3. Color denotes the equivalent stress. Rear facesheets in all the cases except for $v_p = 4$ km/s and $S_r = 27.625$ mm are perforated. Fig. 2(d) shows the final morphology of the configuration $S_r = 27.625$ mm at $v_p = 4$ km/s, where only a bulge can be observed on the rear facesheet.

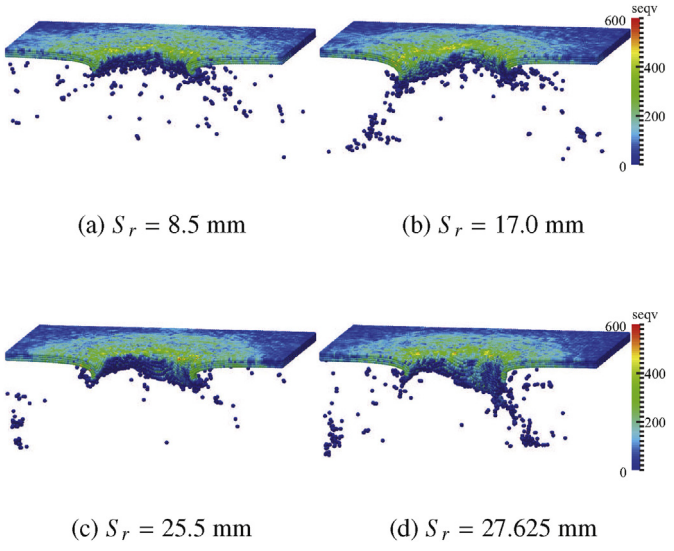

Fig. 3. Morphologies of the rear facesheets at $t = 50$ μs. $v_p = 5$ km/s. (For interpretation of the references to color in this figure citation, the reader is referred to the web version of this article.)

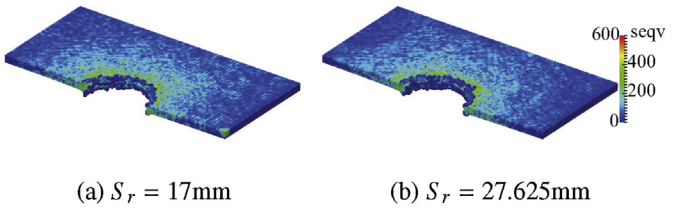

Fig. 4. Final morphologies of the front facesheets. $v_p = 4000$ m/s. (For interpretation of the references to color in this figure legend, the reader is referred to the web version of this article.)

So the shielding performance is much improved without any mass increase but only by movement of the intermediate facesheet.

Morphologies of the front facesheets of $S_r = 17$ mm and $S_r = 27.625$ mm are given in Fig. 4. The holes on the front facesheet are smoother than those on the rear facesheets, and the hole diameters are very close for different S_r. This is because the impact process of the front facesheet is too transient to reflect the influences of honeycomb cores and other facesheets. As discussed in Ref. [11], the hole diameter of front facesheet can be estimated by the hole diameter of hyper-velocity impact on a single plate. Deformations of the intermediate facesheets and their adjacent honeycomb core walls are given in Fig. 5 where the colors indicate different components. The hole diameters of intermediate facesheets do not show obvious difference for different configurations, but deformation patterns of adjacent honeycomb cores are different, which may be an important influential factor for different shielding performance.

To quantitatively describe the shielding performance, the dimensionless hole diameter $\bar{D}_{\text{rear}}$ and the dimensionless mass loss m_l of the rear facesheet are shown in Fig. 6 for 4 km/s and Fig. 7 for 5 km/s. $\bar{D}_{\text{rear}}$ is defined as the hole diameter of the rear facesheet (D_{rear}) divided by d_p. D_{rear} is calculated using the same measurement method considering the cyclic symmetry in every 60° of the honeycomb core proposed in Ref. [11]. m_l is defined as the mass loss during impact divided by the initial mass of the rear facesheet. m_l can describe the damage more accurately, since the damage to the rear facesheet may be in the perforation form or in the bulge form for different configurations. Similar trends can be found for both curves except for a couple of points. One minimum value appears at $S_r = 27.625$ mm for $v_p = 4$ km/s. Two minimums are observed for $v_p = 5$ km/s, which are $S_r = 10.625$ mm and $S_r = 27.625$ mm. Though the rear facesheet is penetrated when $v_p = 5$ km/s and $S_r = 27.625$ mm, an obvious decrease of hole diameter can also be observed compared to the

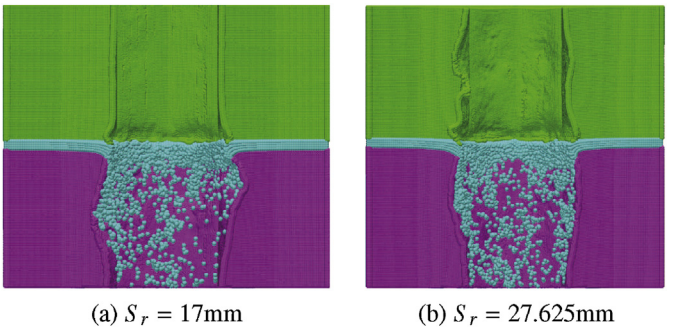

Fig. 5. Final morphologies (front view) of the intermediate facesheets and adjacent honeycomb cores. $v_p = 4000$ m/s. Green denotes the front honeycomb core, light blue denotes the intermediate facesheet, and purple denotes the rear honeycomb core. (For interpretation of the references to color in this figure legend, the reader is referred to the web version of this article.)

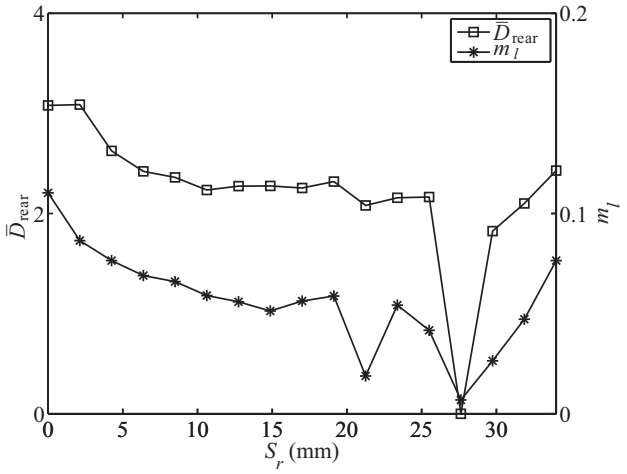

Fig. 6. Dimensionless hole diameter and mass loss of the rear facesheet when v_p = 4 km/s.

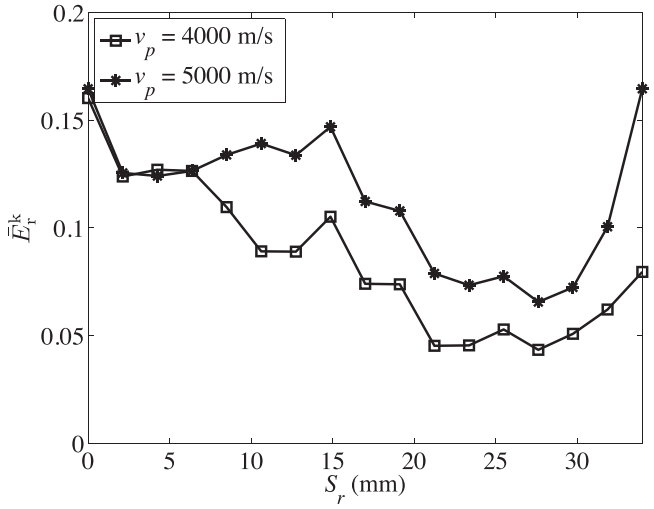

Fig. 8. Dimensionless residual kinetic energy versus S_r.

case where the intermediate facesheet is at the right middle position.

3.2. Residual kinetic energy

The dimensionless residual kinetic energy $\bar{E}_r^k = E_r^k/E_0^k$ is shown in Fig. 8, where E_r^k is the total residual kinetic energy of the shielding structure and the projectile, E_0^k is the total initial kinetic energy. $\bar{E}_r^k$ is used to investigate the shielding performance complementary to D_{rear}/d_p and m_l.

The minimum values of $\bar{E}_r^k$ appear at S_r = 27.625 mm for both $v_p = 4$ km/s and $v_p = 5$ km/s. Though $\bar{D}_{\text{rear}}$ and m_l reach local minimum values at S_r = 10.625 mm when $v_p = 5$ km/s, the residual energy is still high for this configuration. As the functionality of shielding structure is to absorb impact energy, smaller residual energy is highly desired in addition to small perforation holes. The rear facesheet is not perforated when S_r = 27.625 mm for v_p = 4 km/s, but the kinetic energy is also carried by backward-ejected debris so that the residual kinetic energy is not zero.

3.3. Discussion and multilayer improvement

From the above results, shielding performance is best when S_r = 27.625 mm (i.e. S_f = 6.375 mm) as both the hole diameter and the residual energy reach minimum values. The intermediate facesheet should be positioned where its shielding functionality is fully utilized. If the intermediate facesheet is very close to the front facesheet, the debris fragments do not spread enough large range before they impact on the intermediate facesheet, as shown in Fig. 9(a). So the intermediate facesheet will be perforated easily without absorbing enough energy. If the intermediate facesheet is too far away from the front facesheet, most of the debris fragments will expand, be hindered and reside in the area close to cell walls, as shown in Fig. 9(b). The impact intensity on the intermediate and the rear facesheets will still be high.

The intermediate facesheet should be placed where the debris fragments expand right to cell walls. Such distance is defined as the

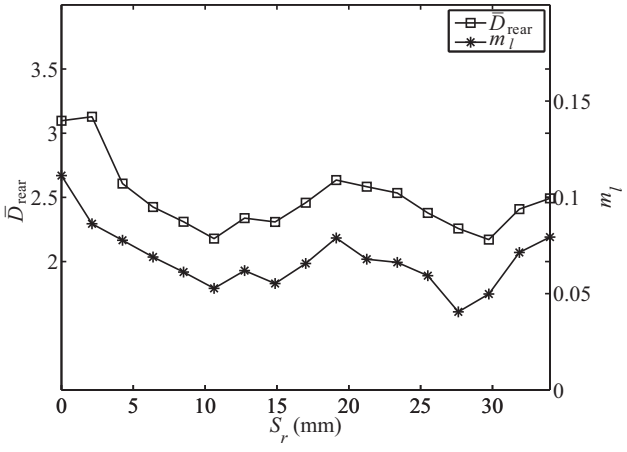

Fig. 7. Dimensionless hole diameter and mass loss of the rear facesheet when v_p = 5 km/s.

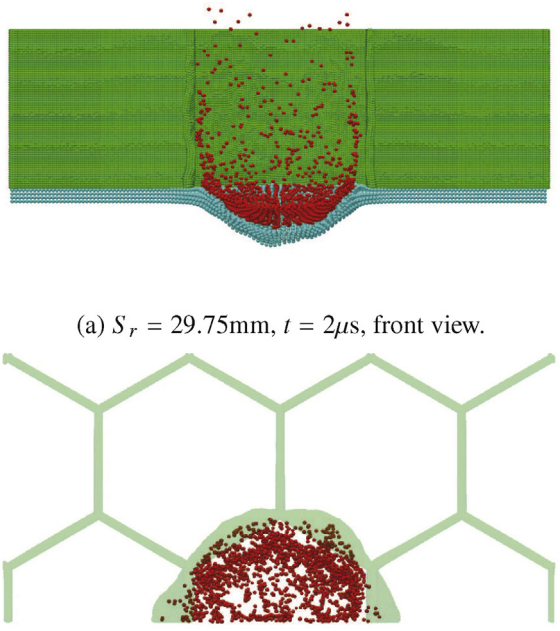

Fig. 9. Typical cases where the intermediate facesheet is (a) too close to the front facesheet or (b) too far away from the front facesheet. v_p = 4000 m/s. Green denotes the honeycomb cores, light blue denotes the intermediate facesheet, and red particles are projectile fragments. (For interpretation of the references to color in this figure legend, the reader is referred to the web version of this article.)

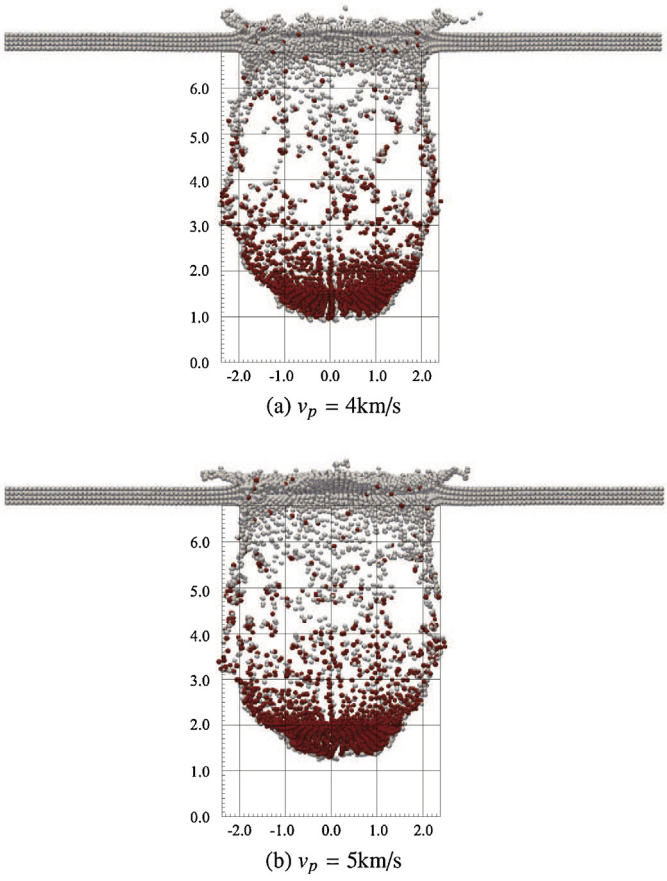

Fig. 10. Calculation of S_{equi} by measuring the distance the fragments have traveled before they occupy the range of one honeycomb cell.

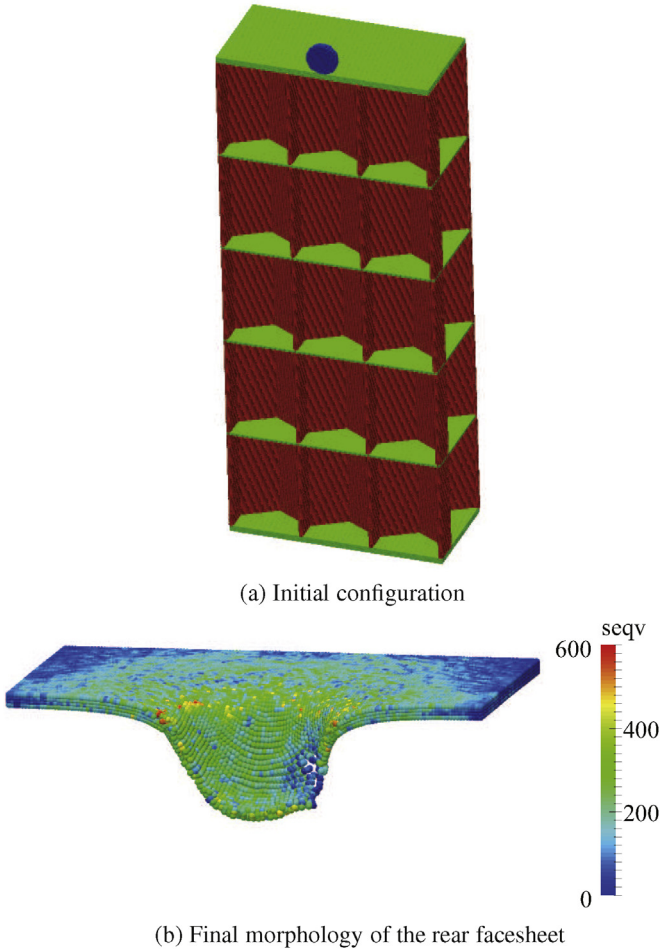

Fig. 11. Multilayer honeycomb panel: Configuration and final morphology of the rear facesheet. Color in the left figure indicates different components; color in the right figure denotes equivalent stress. (For interpretation of the references to color in this figure legend, the reader is referred to the web version of this article.)

equivalent shielding distance (S_{equi}). Lathrop and Sennett proposed a rough estimate $S_{equi} = 2D_{hc}$ for single honeycomb core [19]. More precise value of S_{equi} should rely on t_f and v_p. Two computations with only the front facesheet and $v_p = 4$ km/s and $v_p = 5$ km/s are carried out to find precise S_{equi}. The expansion process of the debris fragments is monitored, and the distance the debris fragments have traveled in the transverse direction before they reach the border of the cell walls is recorded, as shown in Fig. 10. For current examples, S_{equi} is $1.18D_{hc}$ for $v_p = 5$ km/s and $1.26D_{hc}$ for $v_p = 4$ km/s, respectively. Among all the configurations computed above, $S_f = 6.375$ mm ($1.34D_{hc}$) is the closest value to S_{equi}.

The above discussions indicate that $S_f \approx S_{equi}$ can result in the best shielding performance. The existence of intermediate facesheet provides more opportunities for the debris fragments to interact with and then be split by the cell walls to spread wider range. Inspired by the above discussion, a new structure with multiple honeycomb cores is proposed. More intermediate facesheets are inserted and all the intermediate facesheet are placed uniformly. The distance between two adjacent facesheets is around S_{equi}. For the current model, the improved multilayer honeycomb panel has four intermediate facesheets with intervals 6.8 mm ($1.43D_{hc}$), as shown in Fig. 11(a). The thickness of each intermediate facesheet is 0.1 mm, that is, the initial intermediate facesheet is divided into four much thinner facesheets. It should be noted that the total structural weight is *not* increased as the total masses of four intermediate facesheets is equal to the mass of the initial intermediate facesheet.

The results of multilayer honeycomb structure under impact velocity 5 km/s are shown in Fig. 11(b). The rear facesheet is not perforated with only a bulge can be seen. Great improvement is obtained by distributing the intermediate facesheet to construct multiple honeycomb cores, where the height of each core is about S_{equi}.

4. Conclusion

Double honeycomb structures are investigated with the focus on their shielding performance when the position of the intermediate facesheet varies. Point-based internal-structure model and material point method are utilized for large scale simulation. It is found that placing the intermediate facesheet at the right middle of the structure is not the best choice. The intermediate facesheet should be positioned where the height of the front honeycomb core is about the equivalent shielding distance.

A strategy of distributing single intermediate facesheet into several much thinner intermediate facesheets to construct honeycomb panel of multiple cores is proposed. The new structure has much improved shielding property even when the impact velocity is as high as 5 km/s, but the total weight is the same as the original double honeycomb panel.

Other methods improving the shielding capability, for example, the staggered double honeycomb cores [20], can be combined with the above strategies. Improving the shielding performance with new facesheet material, such as fiber reinforced composite, is also under investigation. Double and multiple honeycomb panel can be further improved with considering other functional components.

Investigation on theoretical or empirical formula for equivalent shielding distance is another future research work.

References

[1] K.B. Shin, J.Y. Lee, S.H. Cho, An experimental study of low-velocity impact responses of sandwich panels for Korean low floor bus, Compos. Struct. 84 (2008) 228–240.

[2] V. Crupi, G. Epasto, E. Guglielmino, Comparison of aluminium sandwiches for lightweight ship structures: honeycomb vs. foam, Mar. Struct. 30 (2013) 74–96.

[3] V. Crupi, G. Epasto, E. Guglielmino, H. Mozafari, S. Najafian, Computed tomography-based reconstruction and finite element modelling of honeycomb sandwiches under low-velocity impacts, J. Sandwich Struct. Mater. 16 (4) (2014) 377–397.

[4] A. Akatay, M.O. Bora, O. Çoban, S. Fidan, V. Tuna, The influence of low velocity repeated impacts on residual compressive properties of honeycomb sandwich structures, Compos. Struct. 125 (2015) 425–433.

[5] H. Mozafari, S. Khatami, H. Molatefi, Out of plane crushing and local stiffness determination of proposed foam filled sandwich panel for Korean Tilting Train eXpress – numerical study, Mater. Des. 66 (2015) 400–411.

[6] W. Gong, Y. Liu, X. Zhang, H. Ma, Numerical investigation on dynamical response of aluminum foam subject to hypervelocity impact with material point method, Comput. Modell. Eng. Sci. 83 (5) (2012) 527–545.

[7] B. Castanie, C. Bouvet, Y. Aminanda, J. Barrau, P. Thevenet, Modelling of low-energy/low-velocity impact on Nomex honeycomb sandwich structures with metallic skins, Int. J. Impact Eng. 35 (2008) 620–634.

[8] W. Schonberg, F. Schäfer, R. Putzar, Hypervelocity impact response of honeycomb sandwich panels, Acta Astronaut. 66 (3-4) (2010) 455–466.

[9] R.J. Turner, E.A. Taylor, J.A.M. McDonnell, H. Stokes, P. Marriott, J. Wilkinson, D.J. Catling, R. Vignjevic, L. Berthoud, M. Lambert, Cost effective honeycomb and multi-layer insulation debris shields for unmanned spacecraft, Int. J. Impact Eng. 26 (1) (2001) 785–796.

[10] E.A. Taylor, J.P. Glanville, R.A. Clegg, R.G. Turner, Hypervelocity impact on spacecraft honeycomb: hydrocode simulation and damage laws, Int. J. Impact Eng. 29 (1) (2003) 691–702.

[11] P. Liu, Y. Liu, X. Zhang, Internal-structure-model based simulation research of shielding properties of honeycomb sandwich panel subjected to high-velocity impact, Int. J. Impact Eng. 77 (2015) 120–133.

[12] W.P. Schonberg, F. Schaefer, R. Putzar, Predicting the perforation response of honeycomb sandwich panels using ballistic limit equations, J. Spacecraft Rockets 46 (5) (2009) 976–981.

[13] S. Ma, X. Zhang, X. Qiu, Comparison study of MPM and SPH in modeling hypervelocity impact problems, Int. J. Impact Eng. 36 (2009) 272–282.

[14] P. Huang, X. Zhang, S. Ma, H. Wang, Shared memory OpenMP parallelization of explicit MPM and its application to hypervelocity impact, Comput. Modell. Eng. Sci. 38 (2) (2008) 119–148.

[15] Y. Liu, H.-K. Wang, X. Zhang, A multiscale framework for high-velocity impact process with combined material point method and molecular dynamics, Int. J. Mech. Mater. Des. 9 (2013) 127–139.

[16] P. Liu, Y. Liu, X. Zhang, Investigation on high-velocity impact of micron particles using material point method, Int. J. Impact Eng. 75 (2015) 241–254.

[17] X. Zhang, Y.P. Lian, Y. Liu, X. Zhou, Material Point Method, Tsinghua University Press, Beijing, 2013.

[18] D. Sulsky, S.J. Zhou, H.L. Schreyer, Application of a particle-in-cell method to solid mechanics, Comput. Phys. Commun. 87 (1) (1995) 236–252.

[19] B. Lathrop, R. Sennett, Effects of hypervelocity impact on honeycomb structures, J. Spacecraft Rockets 5 (12) (1968) 1496–1497.

[20] P. Liu, Y. Liu, X. Zhang, Simulation of hyper-velocity impact on double honeycomb sandwich panel and its staggered improvement with internal-structure model, Int. J. Mech. Mater. Des. (2015), http://dx.doi.org/10.1007/s10999-015-9300-7.